



HAL
open science

Synthesis, structural and magnetic properties of $\text{CoCr}_x\text{Fe}_{2-x}\text{O}_4$ ($0.0 \leq x \leq 1.0$) nano-ferrite

Priyanka Tiwari, Shashank Kane, Rulan Verma, Frédéric Mazaleyrat

► **To cite this version:**

Priyanka Tiwari, Shashank Kane, Rulan Verma, Frédéric Mazaleyrat. Synthesis, structural and magnetic properties of $\text{CoCr}_x\text{Fe}_{2-x}\text{O}_4$ ($0.0 \leq x \leq 1.0$) nano-ferrite. *Advances in basic Science (ICABS 2019)*, Feb 2019, Bahal, India. pp.160016, 10.1063/1.5122597 . hal-04452727

HAL Id: hal-04452727

<https://hal.science/hal-04452727>

Submitted on 12 Feb 2024

HAL is a multi-disciplinary open access archive for the deposit and dissemination of scientific research documents, whether they are published or not. The documents may come from teaching and research institutions in France or abroad, or from public or private research centers.

L'archive ouverte pluridisciplinaire **HAL**, est destinée au dépôt et à la diffusion de documents scientifiques de niveau recherche, publiés ou non, émanant des établissements d'enseignement et de recherche français ou étrangers, des laboratoires publics ou privés.

Copyright

RESEARCH ARTICLE | AUGUST 29 2019

Synthesis, structural and magnetic properties of $\text{CoCr}_x\text{Fe}_{2-x}\text{O}_4$ ($0.0 \leq x \leq 1.0$) nano-ferrite

P. Tiwari; S. N. Kane ; R. Verma; F. Mazaleyrat

 Check for updates

AIP Conf. Proc. 2142, 160016 (2019)

<https://doi.org/10.1063/1.5122597>



CrossMark



Cut Hall measurement time in *half* using an M91 FastHall™ controller



Also available as part of a tabletop system and an option for your PPMS® system

Synthesis, Structural and Magnetic Properties of $\text{CoCr}_x\text{Fe}_{2-x}\text{O}_4$ ($0.0 \leq x \leq 1.0$) Nano-Ferrite

P. Tiwari^{1,2}, S. N. Kane^{1, a)}, R. Verma¹ and F. Mazaleyrat³

¹Magnetic Materials Laboratory, School of Physics, D. A. University, Khandwa road, Indore – 452001, India.

²Department of Physics, Prestige Institute of Engineering Management and Research, Indore - 452010, India.

³SATIE, ENS Universite Paris-Saclay, CNRS 8029, 61 Av. du Pdt. Wilson, F-94230, Cachan, France.

^{a)}Corresponding author: kane_sn@yahoo.com

Abstract. Present study reports, effect of Cr addition on structural, magnetic properties of $\text{CoCr}_x\text{Fe}_{2-x}\text{O}_4$ ($0.0 \leq x \leq 1.0$) ferrites, synthesized by sol-gel auto combustion method. X-ray diffraction (XRD), vibrating sample magnetometer (VSM) were utilized to monitor the modification of structural, magnetic properties, and correlation between them. Scherrer's grain diameter ranging between 14.7 nm - 26.2 nm. Coercivity (H_c) and anisotropy constant (K_1) values respectively ranges between 1249- 700 Oe and 20.01×10^4 to 1.01×10^4 erg/cc. Best magnetization value of $56.77 \text{ Am}^2/\text{kg}$ was obtained for $x = 0.44$. Variation of magnetic properties can be understood in terms of Cr-addition induced re-distribution of cations. Coercivity (H_c) dependence with grain size, shows that studied samples lie in the region with overlap between single and multi-domain region.

INTRODUCTION

Spinel ferrites with general formula $\text{Me}^{2+}\text{O}.\text{Fe}^{3+}_2\text{O}_3$ (where Me represents divalent ion), are technologically important owing to their interesting electrical, and magnetic properties [1]. They exhibit fcc structure belongs to space group Fd3m. Spinel lattice consisting of 32 anions forms closed pack structure with 64 tetrahedral (*site-A*) and 32 octahedral (*B-site*) out of which 8 and 16 are occupied by metal ions. Soft spinel ferrites (Fd₃ m space group) exhibit fcc structure with 64 tetrahedral (*A*) and 32 octahedral (*B*) sites. It is worth noting that, substitution of a magnetic or a non-magnetic cation modifies the cationic distribution on A, B site, and thus would affect the magnetic interactions, which in-turn will influence the magnetic properties [2]. Variation in structural, magnetic properties can be achieved via: partial or complete substitution; a particular synthesis method; thermal treatment etc.

Cobalt ferrites show remarkable properties, and thus have been extensively used in electronic devices [3,4], Magnetic Resonance Imaging (MRI), Targetted drug delivery, Hyperthermia for cancer treatment [5,6], high density storage devices, magnetic fluids [7,8], transformer cores, microwave devices, humidity, and gas sensors, etc. Substitution of elements such as Chromium in Cobalt ferrites has been proposed, in order to tailor the magnetic, and magneto mechanical properties of these materials. Chromium substituted Cobalt ferrites are of particular interest in which the Cr^{3+} ions are reported to have a strong preference for the B sites (Octahedral) of the spinel structure of the ferrites [8,9]. Substitution of Cr^{3+} ions ($3\mu_B$) for Fe^{3+} ions ($5\mu_B$) will have effect on structural, magnetic properties of Co-Cr based ferrites. Chromium (Cr^{3+}) ions with antiferromagnetic nature are renowned for achieving control over structural and magnetic parameters in developing technologically important materials, and are of use in various applications including: in high frequency devices, in catalysis activity, sensors because of their low hysteresis losses and higher coercivity [9]. Selective and, or successive Cr addition (for Fe^{3+} ion) into-ferrite can also be effectively utilized to curie temperature of the Co-Cr based ferrites. Sol gel auto combustion is one of the best method to synthesize ferrites. A distinct advantage of sol-gel method is that the final phase formation can be achieved even in 'dry-gel' form so would have better control over grain diameter [10], but information available on the spinel phase formation in dry gel form for Cr^{3+} substituted ferrite is less explored in literature. Therefore, present work reports synthesis of $\text{CoCr}_x\text{Fe}_{2-x}\text{O}_4$ ($0.0 \leq x \leq 1.0$) ferrites, by sol gel auto-combustion method (*where no heat treatment was used*), utilizing XRD and magnetic measurements to probe structural, magnetic properties.

EXPERIMENTAL DETAILS AND DATA ANALYSIS

Sol-gel auto-combustion method was used to synthesize $\text{CoCr}_x\text{Fe}_{2-x}\text{O}_4$ spinel ferrites. Samples were prepared by using AR grade nitrate/citrate precursors: Chromium nitrate ($\text{Cr}(\text{NO}_3)_3 \cdot 9\text{H}_2\text{O}$), Cobalt nitrate ($\text{Co}(\text{NO}_3)_2 \cdot 6\text{H}_2\text{O}$), Ferric nitrate – ($\text{Fe}(\text{NO}_3)_3 \cdot 9\text{H}_2\text{O}$) in stoichiometric ratio. The precursors were dissolved in 10 ml de-ionized water keeping metal salt to citric acid ratio as 1:1, maintaining pH of the solution at 7 by adding ammonia solution (NH_4OH). Resulting solution was heated at $\sim 110^\circ\text{C}$ to obtain fluffy powder, called as ‘burnt powder’ which was used for structural [10], magnetic measurements. Room temperature x-ray diffraction (XRD) patterns of the synthesized $\text{CoCr}_x\text{Fe}_{2-x}\text{O}_4$ ferrite samples were recorded in θ - 2θ configuration via Bruker D8 advanced diffractometer CuK_α radiation (wavelength: 0.15406 nm), equipped with Bruker Lynx Eye detector. The lattice parameter (a_{exp}) corresponding to [311] reflection was obtained by expression: $a_{\text{exp}} = d\sqrt{h^2 + k^2 + l^2}$, where d – inter-planer spacing and, (h, k, l) - miller indices. a_{exp} was used to obtain the x-ray density (ρ_{XRD}) of the studied samples. Particle size (D) was obtained by using Scherer’s equation: $D = 0.9\lambda / \beta \cos\theta$, where Specific surface area (S) was calculated using the expression: $S = [6 / (D \times \rho_{\text{XRD}})]$, where D - particle size and ρ_{XRD} - x-ray density. In the present study, (220) (422) (400) (440) planes are considered for cation distribution as these planes are sensitive to distribution of cations among tetrahedral A , octahedral B sites of the spinel lattice, reflections employing Bertaut method [11]. The calculated, observed intensity ratios were compared for several combinations of cation distribution at A, B-sites. Obtained cation distribution was used to calculate, Néel magnetic moment (theoretical magnetization at 0 K ‘ $M_{s(0)}$ ’), is calculated using formula: $n_N = M_B - M_A$ in Bohr magneton (μ_B) where M_A is magnetic moment of A-site and M_B is magnetic moment of B-site, oxygen position parameter (u), bond angles ($\theta_1, \theta_2, \theta_3, \theta_4, \theta_5$), and inversion parameter (δ). Canting angle $\alpha_{\text{Y-K}}$ was also calculated. Hysteresis measurements were done by Lakeshore VSM Model 7410 by applying maximum field: $H_{\text{max}} \approx 1.9\text{ T}$. Coercivity (H_c), saturation magnetization (M_s) and, anisotropy constant (K_1), static magnetic losses were obtained from Hysteresis measurements.

RESULTS AND DISCUSSIONS

Figure 1, represents the XRD pattern of all the samples of $\text{CoCr}_x\text{Fe}_{2-x}\text{O}_4$ ($0.0 \leq x \leq 1.0$) nano ferrite. Presence of characteristic peaks from (220), (311), (222), (400), (422), (511), and (440) planes of ferrite structure confirm the presence of single phase with fcc structure (Fd_3m space group) without any impurity. Table 1 depicts the structural parameters: Lattice parameter (a_{exp}), unit cell volume (V), X-ray density (ρ_{XRD}), specific surface area (S) obtained by analyzing XRD.. Observed linear decrease of a_{exp} , D_s , V with increasing Cr^{3+} content, attributed to the slight decrease of ionic radius of the substituent Cr^{3+} (0.064 nm) as compared to the Fe^{3+} (0.067 nm) ion which is being substituted [12]. Volume of unit cell (V) varies between 0.5894 - 0.5874 nm^3 . The average Scherrer’s grain diameter (D) of the studied samples estimated from most intense peak [311] varies between 05.4 – 26.2 nm , shows noticeable lower grain size confirms the formation of nano crystalline ferrites [13]. The variation of X-ray density (ρ_{XRD}) found to be decreases (5218.2 – 5287.1 kg/m^3) with increasing Cr^{3+} content. This variation is ascribed due to the replacement of heavier Fe^{3+} atoms (with higher atomic weight of $\text{Fe}^{3+} = 55.84\text{ gm/mole}$) by lighter Cr^{3+} atoms (with lesser atomic weight of $\text{Cr}^{3+} = 51.99\text{ gm/mole}$). Specific surface area of the studied samples varies between 43.22 – $78.03\text{ m}^2/\text{g}$.

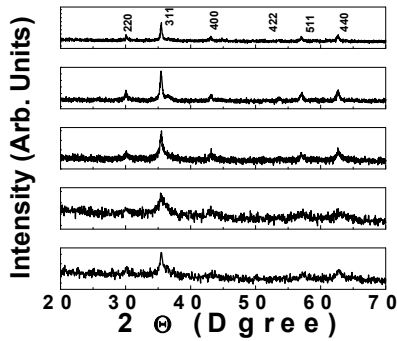


FIGURE 1. XRD patterns of the studied samples.

x	a_{exp}	D_s	ρ_{XRD}	V	S
	nm	(nm)	(kg/m^3)	(nm^3)	(m^2/g)
0.0	0.8384	26.2	5287.2	0.5894	43.22
0.11	0.8388	22.0	5258.5	0.5901	51.64
0.22	0.8383	16.6	5246.2	0.5891	68.76
0.33	0.8351	05.4	5283.2	0.5825	212.26
0.44	0.8372	14.7	5218.1	0.5874	78.03

Table 2. Cation distribution (for A, B site), inversion parameter (δ), experimental, theoretical lattice parameter (a_{exp} , a_{Th}), oxygen position parameter (u^{43m}) of $CoCr_xFe_{2-x}O_4$ as a function of Cr content.

X	Cation distributions	δ	a_{exp} (nm)	a_{Th} (nm)	u^{43m}
0.00	$(Co^{2+}_{0.75}Fe^{3+}_{0.25})^A[Co^{2+}_{0.25}Fe^{3+}_{1.75}]^B$	0.25	0.8384	0.8385	0.3834
0.25	$(Co^{2+}_{0.5}Cr^{3+}_{0.2}Fe^{3+}_{0.3})^A[Co^{2+}_{0.5}Cr^{3+}_{0.05}Fe^{3+}_{1.45}]^B$	0.3	0.8388	0.8388	0.3835
0.50	$(Co^{2+}_{0.5}Cr^{3+}_{0.15}Fe^{3+}_{0.35})^A[Co^{2+}_{0.5}Cr^{3+}_{0.35}Fe^{3+}_{1.15}]^B$	0.35	0.8383	0.8377	0.3831
0.75	$(Co^{2+}_{0.5}Cr^{3+}_{0.1}Fe^{3+}_{0.4})^A[Co^{2+}_{0.5}Cr^{3+}_{0.65}Fe^{3+}_{0.85}]^B$	0.4	0.8351	0.8366	0.3832
1.00	$(Co^{2+}_{0.2}Cr^{3+}_{0.35}Fe^{3+}_{0.45})^A[Co^{2+}_{0.8}Cr^{3+}_{0.65}Fe^{3+}_{0.55}]^B$	0.45	0.8372	0.8372	0.3831

Table 2 depicts the cation distribution, oxygen positional parameter (u), inversion parameter (δ), experimental, theoretical lattice parameter (a_{exp} , a_{th}) for the studied samples. Perusal of table 2 shows that with Cr^{3+} ion addition: concentration of Fe^{3+} ions decreases on B site, whereas the concentration of Co^{2+} , Cr^{3+} ions on B site systematically increases, which should mirror in magnetic properties (especially in saturation magnetization values). u^{43m} values show minor changes in oxygen displacement, displaying distortion in the spinel structure, which even will affect magnetic properties. Good matching of a_{exp} a_{th} shows that the obtained cation distribution is close to reality. Inversion parameter (δ) also gets affected with Cr^{3+} addition and the samples become more mixed spinel nature.

Table 3 shows the variation in ionic-radii of A-site (r_A) and B-site (r_B), shared tetrahedral edge (d_{AE}), shared octahedral edge (d_{BE}), unshared octahedral edge (d_{BEU}). In the studied samples r_A , r_B respectively varies between 0.0550 nm – 0.0559 nm, and 0.0645 - 0.0646, which is comparable with ionic radii of Co^{2+} , Cr^{3+} , so with successive Cr^{3+} addition, there is not much change in r_A , r_B . Observed changes in r_A , r_B are consistent with d_{AE} , d_{BE} , d_{BEU} values, which will have effect on both structural and magnetic properties.

Figure 2, illustrate the variation of the bond angles (θ_1 , θ_2 , θ_3 , θ_4 , θ_5) as a function of Cr^{3+} . It is worth noting that, strength of the magnetic interactions ($A-O-B$, $B-O-B$ and $A-O-A$) is directly proportional to the bond angle [14]. The bond angles θ_1 , θ_2 , represent the angles between $A-O-B$, bond angles θ_3 , θ_4 , represent angles between $B-O-B$ and θ_5 represents angles between $A-O-A$, thus representing B-B, B-B and A-A interaction. Observed trend of bond angles θ_1 , θ_2 , θ_3 , θ_4 and θ_5 , for x up to 0.50 indicate strengthening of A–B interaction, and weakening of B–B, A–A interaction. Beyond x = 0.5, obtained behavior of bond angles θ_1 , θ_2 , θ_3 , θ_4 and θ_5 , depicts weakening of, B–B interaction, whereas A–B, A–A interaction strengthens, which affects magnetic properties. Figure 3 a, shows similar trend of experimental M_s at 300 K (obtained from VSM measurements) and that of theoretical magnetization at 0 K: $M_{s(0)}$, shows that the magnetic behavior of the studied annealed samples obeys

Table 3: Variation in ionic-radii of A-site (r_A) and B-site (r_B), shared tetrahedral edge (d_{AE}), shared octahedral edge (d_{BE}), unshared octahedral edge (d_{BEU}) with Cr content

X	r_A (nm)	r_B (nm)	d_{AE} (nm)	d_{BE} (nm)	d_{BEU} (nm)
0.0	0.0558	0.0646	0.3163	0.2764	0.2967
0.25	0.0559	0.0646	0.3166	0.2764	0.2969
0.5	0.0553	0.0645	0.3156	0.2771	0.2967
0.75	0.0557	0.0645	0.3146	0.2758	0.2955
1.0	0.0550	0.0645	0.3151	0.2768	0.2963

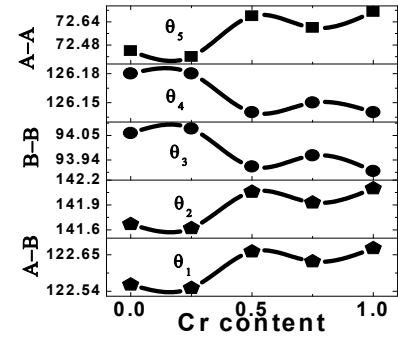


Figure 2. Cr-content dependence of V bond angles (θ_1 , θ_2 , θ_3 , θ_4 , θ_5).

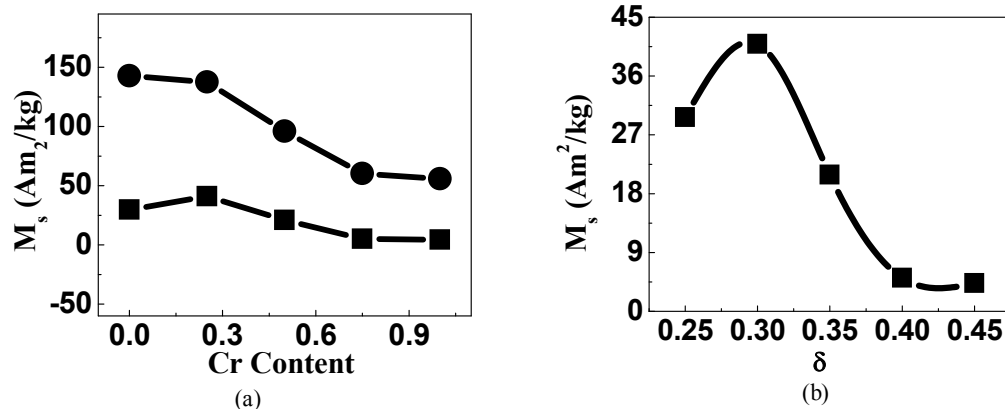


Figure 3: (a) Variation of $M_{s(\text{exp.})}$, $M_{s(\text{th})}$ with Cr content, (b) Variation of M_s with inversion parameter δ .

Néel model [15]. Perusal of figure 2 b shows variation of M_s with inversion parameter δ . With increasing Cr^{3+} doping, Co^{2+} ions, Fe^{3+} ions, and Cr^{3+} ions are distributed on both A, B site, depicting changes in δ , and thus affecting M_s .

Table 4, shows coercivity (H_c), experimental saturation magnetization (M_s), magnetization at 0K ($M_{s(0K)}$), magnetic losses (static), magneto-crystalline anisotropy (K_1), and Yaffet Kittle angle (α_{Y-K}) angle for the studied samples. Perusal of table 4 shows with increasing Cr^{3+} content all the parameters get affected, thus Cr content can be used to tailor magnetic properties of Co-Cr based ferrites. With Cr^{3+} addition, reduction of losses, shows softer magnetic behavior (although M_s values are also considerably affected). Observed changes in α_{Y-K} is also responsible for obtained changes in M_s . Obtained M_s and H_c values are consistent with calculated K_1 values.

Figure 4 a, shows the room temperature hysteresis loop for $\text{CoCr}_x\text{Fe}_{2-x}\text{O}_4$ ferrite as a function of Cr^{3+} content, displaying changes in H_c and M_s .

Figure 4b depicts Cr^{3+} content dependence of anisotropy. Perusal of figure 4 b, decrease in K_1 can be described in the arrangement of single ion anisotropy model. According to this model, Fe^{3+} ions on A and B sites contribute to anisotropy energy. K_1 is then specified by relative combination of Fe^{3+} ions at A site (positive anisotropy) which is compensated by Fe^{3+} ions at B site (negative anisotropy) [16]. With Cr^{3+} doping, cationic re-distribution of Fe^{3+} ions yields different concentrations of Fe^{3+} ions on A, B sites, and thus affects K_1 .

Figure 4 c, depicts, dependence of H_c with Cr addition, whereas inset shows the variation of H_c with grain diameter (D). Perusal of fig. 4 c shows that Cr-addition leads to reduction of H_c , depicting softer magnetic behavior, although H_c increases for $\text{Cr} = 1.0$, which consistent with small increase of K_1 . Inset of figure 4 c shows linear variation of coercivity (H_c), grain size, displays that studied samples lie in the region with overlap between single and multi-domain region as also was suggested earlier [14,16].

Table 4. Coercivity (H_c), experimental saturation magnetization (M_s), magnetization at 0K ($M_{s(0K)}$), static magnetic losses, magneto-crystalline anisotropy (K_1) and Yaffet- Kittle angle (α_{Y-K}) (obtained from cation distribution) for Co-Cr nano-ferrite.

X	H_c (Oe)	$M_{s(\text{exp})}$ (Am ² /kg)	$M_{s(0K)}$ (Am ² /kg)	Losses (J/kg)	$K_1 \times 10^4$ (erg/cc)	$\alpha(Y-K)$ (°)
0.00	1249.0	29.7	142.8	11.10	20.01	60.01
0.25	983.78	40.9	137.4	12.03	27.58	57.41
0.50	714.43	20.9	96.0	4.71	8.08	55.33
0.75	700.16	5.1	60.3	1.01	1.91	49.80
1.00	1016.0	4.3	55.7	1.17	2.34	54.00

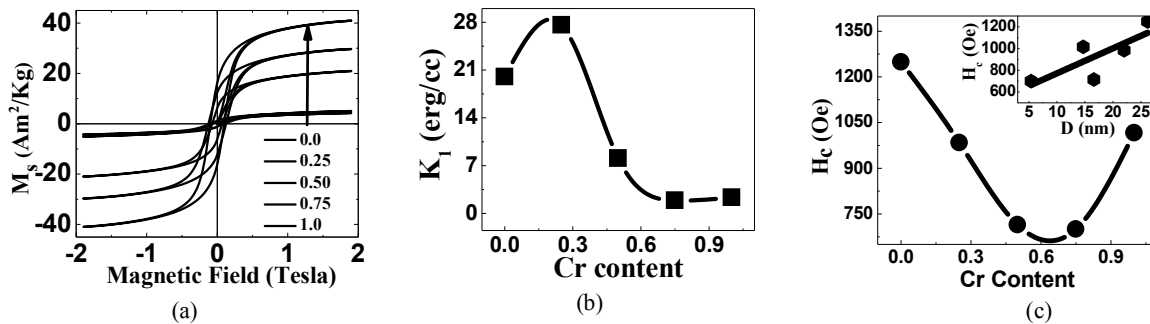


FIGURE 4.(a) Hysteresis loops for Co-Cr ferrite (b) Variation of K_1 with Cr content, (c) Linear variation of H_c with D .

SUMMARY

To summarize sol-gel auto-combustion method was used to synthesize Cr doped Co nano-ferrite: $\text{CoCr}_x\text{Fe}_{2-x}\text{O}_4$ ($0.0 \leq x \leq 1.0$). XRD reveals the formation of pure spinel structure. Grain diameter (D) varies between 14.7 – 26.2 nm. Cr addition shows considerable changes in structural properties. Co^{2+} , Cr^{3+} , and Fe^{3+} ions remain distributed on both A, B site, and Cr^{3+} addition leads to modification of their distribution on A, B site, leads to changes in magnetic properties (showing softer magnetic behavior) via changes in A-b, B-B, A-B interaction.

ACKNOWLEDGMENTS

Authors thank Dr. M Gupta, UGC-DAE CSR, Indore for XRD measurements. S. N. Kane acknowledges gratefully one month hospitality as invited professor at ENS, University Paris-Saclay (France) during June 2018.

REFERENCES

1. S. N. Kane, S. Raguwanshi, M. Satalkar, V. R. Reddy, U. P. Deshpande, T. R. Tatarchuk and F. Mazaleyrat, *AIP Conf. Proc.* **1953**, 030089-4 (2018).
2. J. Smit, H. P. J. Wijn, *Ferites*, Philips Technical Library, Eindhoven, (1959).
3. T. Tatarchuk, M. Bououdina, W. Macyk, O. Shyichuk, N. Paliychuk, I. Yaremiy, B. Al-Najar and M. Pacia, *Nanoscale Res. Lett.* **12**, 141-11 (2017).
4. S. Raghuvanshi, F. Mazaleyrat, and S. N. Kane, *AIP Advances* **8**, 047804–1-047804-11 (2018).
5. D. R. Mane, S. Patil, D. D. Birajdar, A. B. Kadam, S. Shirsath and R. H. Kadam, *Mater. Chem. Phys.*, **126**, 755–760 (2011).
6. R. Verma, S. N. Kane, S. Raghuvanshi, M. Satalkar, S. S. Modak and F. Mazaleyrat, *AIP Conf. Proc.* **1953**, 030135-1-030135-4 (2018).
7. R. G. Kharabe, R. S. Devan, C M. Kanamadi and B. K. Chougule, *Smart Mater. Strut.* **15**, N36–N39 (2006).
8. S. Panchal, S. Raghuvanshi, K. Gahlot, F. Mazaleyrat and S. N. Kane, *AIP Advances* **6**, 055930–6 (2016).
9. S. N. Kane and M. Satalkar, *J. Mater. Sci.* **52**, 3467–3477 (2017).
10. A. Sutka and G. Mezinskis, *Front. Mater. Sci.* **6(2)**, 128–141 (2012).
11. F. Bertaut, *C. R. Acad. Sci.* **230**, 213 (1950).
12. M. M. Hessian, *Journal of Magnetism and Magnetic Materials*, **320**, 2800–2807 (2008). L. Gastaldi and A. Lapicciarella, *J. Solid State Chem.* **30**, 223 (1979).
13. L. Lutterotti and P. scardi, *J. Appl. Cryst* **23**, 246-252 (1990).
14. A. Kolhatkar, A. C. Jamison, D. Litvinov and T. R. Lee, *Int. J. Mol. Sci.* **14(8)**, 15977–16009 (2013).
15. M. Rahimi, M. Eshraghi, and P. Kamel, *Ceramics International*, **40**, 15569–15575 (2014).
16. S. R. Bainade, C. M. Kale, M. C. Sable, *J Supercond Nov Magn.* **31**, 387–394 (2018).